Microwave Photon-Number Amplification

R. Albert,[1] J. Griesmar,[2] F. Blanchet,[1] U. Martel,[2] N. Bourlet[,2] and M. Hofheinz[2,1]

[1]*Université Grenoble Alpes, CEA, INAC-PHELIQS, F-38000 Grenoble, France*
[2]*Institut Quantique, Université de Sherbrooke, Sherbrooke, Québec J1K 2R1, Canada*

We experimentally demonstrate a microwave photon-multiplication scheme which combines the advantages of a single-photon detector and a power meter by multiplying the incoming photon number by an integer factor. Our first experimental implementation achieves an $n = 3$-fold multiplication with 0.69 efficiency in a 116 MHz bandwidth up to an input photon rate of 400 MHz. It loses phase information but does not require any dead time or time binning. We expect an optimized device cascading such multipliers to achieve number-resolving measurement of itinerant photons with low dark count, which would offer new possibilities in a wide range of quantum-sensing and quantum-computing applications.

Quantum-limited power meters able to measure weak signals from single to few photons are not yet available in the microwave domain, hindering measurement of photon number in itinerant quantum states. On the one hand, recent single-photon detectors [1–6] accurately detect single photons, but are intrinsically nonlinear with their binary outcome mapping all incoming nonzero photon number states to the same output state. This noninvertible behavior discards more information than strictly required by commutation relations, in particular, the actual photon number. Many implementations also require frequent resets or use of a latching mechanism, so that even more information on the incoming photon state is lost, e.g., its actual arrival time. On the other hand, more linear watt meters, such as bolometers [7–9], are too noisy to accurately detect single microwave photons.

Instead of power meters, the most common and versatile quantum measurement devices for weak signals in the microwave domain are currently quantum-limited amplifiers [10–12]. Those linear amplifiers are able to amplify signals irrespectively of their phase, but in that case must add amplitude noise. This noise is due to the fact that the quadratures of the electromagnetic field do not commute and, therefore, cannot be accurately measured at the same time. In order to respect the commutation relations of incoming and outgoing fields, the amplifier must couple the signal mode to at least one additional idler mode [13,14]. The zero-point fluctuations of this mode then appear as

additional noise in the amplified signal. This added quadrature noise can be reduced and even avoided if the amplification is made phase sensitive, i.e., only one quadrature is amplified and the other attenuated by the same factor [14], so that phase-space volume is preserved. However, in both cases, those amplifiers effectively measure amplitudes, which do not commute with the photon-number operator. This makes any linear amplifier unable to accurately count propagating photons in the quantum regime.

In this work we instead experimentally demonstrate a phase-insensitive linear photon-number amplification scheme. It is reminiscent of a phase-sensitive amplifier in that it deamplifies phase information, so that phase-space volume is preserved and no noise needs to be added. However, instead of a quadrature, it amplifies photon number and, thereby, allows us to measure the intensity of weak signals with unknown phase by multiplying their photon-number by a factor n. This device is a generalization of a binary single-photon detector which would correspond to the limit $n \to \infty$, where any incoming signal containing more than one photon saturates the device. In the $n = 1$ case, it implements parametric frequency conversion without photon gain, akin to parametric down-conversion.

We implement this photon-number amplifier using Josephson photonics [15–21] based on inelastic Cooper pair tunneling [22,23]. Our device consists of a voltage-biased Josephson junction of energy E_J coupled to input and output transmission lines via two low-Q cavities with resonance frequencies ν_{in} and ν_{out}, and decay rates $\gamma_{\text{in}}, \gamma_{\text{out}}$, respectively [see Fig. 1(a)]. The Josephson junction is biased at a voltage V such that $2eV + h\nu_{\text{in}} = nh\nu_{\text{out}}$, where n is the multiplication factor of the device. Under this condition a photon in the input mode at ν_{in} can be converted into n photons in the output mode at ν_{out}, with a tunneling
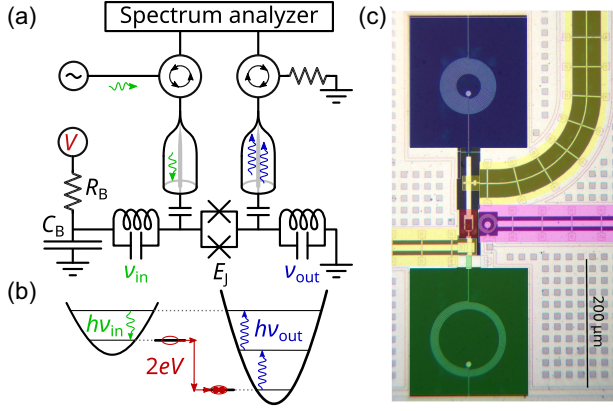
FIG. 1. Setup, sample, and working principle. (a) The sample consists of two buffer resonators at frequencies $\nu_{in} = 4.8$ GHz and $\nu_{out} = 6.13$ GHz. The resonators are nonlinearly coupled by a SQUID biased at a voltage V via a heavily filtered bias line. Its source impedance is modeled by a $R_B = 5$ Ω resistor at an effective temperature of 90 mK. An on-chip capacitor $C_B \approx 100$ pF shunts R_B at the operation frequency (see Appendix A for more details). (b) Schematics of the energy balance for the $n = 2$ conversion process. (c) Optical micrograph of the photomultiplier device. The input and output transmission lines are highlighted in yellow, the SQUID in red, the flux bias line in purple, and the input (output) resonator in green (blue). The large spirals provide the inductance of the input and output modes, thus allowing for high characteristic impedance modes.

Cooper pair providing the difference in energy $2eV$, as seen in Fig. 1(b).

A theoretical model describing this system [17] allows us to calculate the probability T for an incoming photon to be converted to n outgoing photons. On resonance, when $\nu = \nu_{in}$, it is

$$T = \frac{4|\epsilon_n|^2}{(1 + |\epsilon_n|^2)^2}, \tag{1}$$

with

$$|\epsilon_n| = \frac{E_J}{\hbar\sqrt{\gamma_{in}\gamma_{out}}} \frac{1}{\sqrt{n!n}} g_{in} g_{out}^n e^{-(g_{in}^2 + g_{out}^2)/2}, \tag{2}$$

where $g_{in/out} = \sqrt{\pi Z_c^{in/out}/R_Q}$, Z_c being the characteristic impedances of the resonances and $R_Q = h/4e^2$ the superconducting resistance quantum. We thus expect perfect photomultiplication of all incoming photons for $|\epsilon_n| = 1$. This condition, which corresponds to matching the coupling rate between the resonator and the input transmission line with the nonlinear coupling through the junction, can theoretically always be reached by adjusting E_J. This matching enables the device to operate on itinerant photon states. Similar number-resolving detectors have so far only been implemented for photons residing in cavities [24,25], a significantly simpler quantum

measurement problem where the quantum state can be measured several times.

The experimental setup is presented in Fig. 1(a), and a micrograph of the device in Fig. 1(c). The device is made out of a trilayer of Nb-Al/AlO$_x$-Nb, which is used to form Josephson junctions, and the full trilayer stack is also used as one of the routing layers [26]. A second routing layer, made from Nb and separated from the first one by a SiN layer, allows for wire crossings and large capacitors. The two low-Q cavities are realized by planar spiral LC resonators visible in the optical micrograph of Fig. 1(c). They are used to achieve large inductance together with low spurious capacitance. Their resonances are centered at $\nu_{in} = 4.8$ GHz and $\nu_{out} = 6.13$ GHz and have characteristic impedances $Z_c \approx 400$ Ω. These two resonators (input and output) are capacitively coupled to microwave transmission lines. The coupling capacitors are designed to obtain associated coupling rates around $\gamma_{in} \approx \gamma_{out} \approx 90$ MHz. A SQUID, made from two Nb-Al-AlO$_x$-Nb junctions, acts as a single Josephson junction with Josephson energy $E_J(\Phi)$, tunable *in situ* by a local magnetic flux Φ (purple line). While we did not directly measure the critical current of that particular device, due to the voltage noise such a measurement would add, we can estimate its value using test Josephson junctions fabricated on the same wafer. We thus estimate the maximum critical current of our SQUID to be $I_c^{max} \approx 60$ nA, or equivalently $E_J^{max} \approx 120$ μeV. The flux bias lines are low-pass filtered at dilution temperature with homemade lossy transmission-line filters [27]. A dc voltage bias is applied to the SQUID via a 5 Ω/1 MΩ voltage divider with heavy low-pass filtering [26]. The device was measured in a dilution cryostat with a base temperature of $T \approx 10$ mK. More information on the setup can be found in Appendix A.

Figure 2 shows the power spectral density (PSD) of spontaneous emission from the device cooled down to $T \approx 10$ mK. For this measurement, no microwave tone is applied to the photomultiplier. Only a dc voltage bias, expressed in terms of its Josephson frequency $\nu_J = 2eV/h$, and a magnetic flux are applied. At maximal SQUID frustration $\Phi = \Phi_0/2$ [see Fig. 2(a)], only emission close to the input (4.8 GHz) and output (6.13 GHz) modes is visible. In this panel, the PSD of both the input (blue) and output (green) resonator is represented. The brightest spots around $\nu_J = 4.8$ and 6.13 GHz are on the $\nu_J = \nu$ line and correspond to the emission of one photon per tunneling Cooper pair in the corresponding resonator. The emission of two photons per tunneling Cooper pair is also visible near the $\nu_J = 2\nu$ line. The last two spots around $\nu_J = \nu_{in} + \nu_{out} \approx 11$ GHz correspond to the emission of one photon in each resonator per tunneling Cooper pair.

Figures 2(b) and 2(c) show the emission rate of the input and output resonators, integrated over a 400 MHz bandwidth centered at, respectively, the input and output resonance frequencies, indicated by horizontal dashed lines
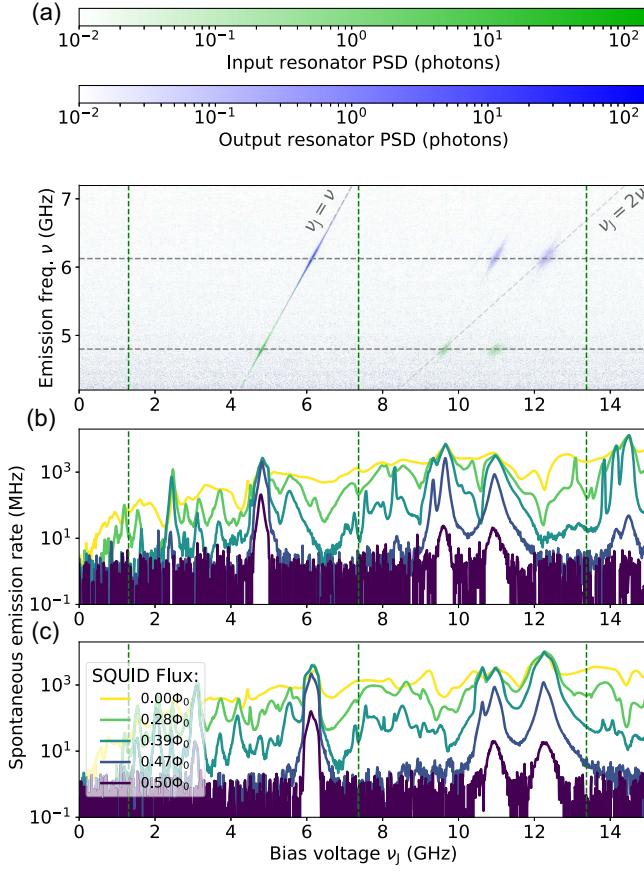
FIG. 2.   Spontaneous emission. (a) Power spectral density (PSD) as a function of emission frequency and bias voltage. The PSD for the input (output) resonator is plotted in shades of green (blue). The flux in the SQUID loop is set to $\Phi_0/2$ to minimize the Josephson energy. (b),(c) Photon emission rate from the input and output resonator, respectively, integrated over a 400 MHz bandwidth centered at 4.8 GHz (input) and 6.13 GHz (output) for 5 values of flux in the SQUID loop. These frequencies are represented by horizontal dashed gray lines in (a). The flux values of $0.47\Phi_0$, $0.39\Phi_0$, and $0.28\Phi_0$ correspond to the dashed vertical lines in Fig. 3 and the flux used in Fig. 4. The three vertical green dashed lines correspond, from left to right, to the voltages used for the conversions of Figs. 3 and 4 with, respectively, $n = 1$, 2, and 3.

in Fig. 2(a). The lines for $\Phi = \Phi_0/2$ show the well-defined processes discussed above. At larger Josephson energies (fluxes closer to 0), the emission peaks are less well resolved as more and more complex processes emerge. At the highest Josephson energy, higher order processes involving several Cooper pairs and photons in many modes give rise to emission at nearly all bias voltages.

We then bias the SQUID at voltages V such that $h\nu_{in} + 2eV = nh\nu_{out}$, which enables the multiplication of photons in our device. The voltages corresponding to $n = 1$, 2, and 3 are indicated by vertical dashed lines in Fig. 2. When a microwave tone at frequency ν is applied at the input of the device, the desired converted signal appears centered at a frequency $\nu_{conv} = \nu_{out} + (\nu - \nu_{in})/n$. For

$n = 1$, its bandwidth will be small, mainly set by low-frequency fluctuations of the dc voltage. For $n > 1$, the converted photons will be spread over the much larger bandwidth of the output resonator [17]. We measure this converted signal by integrating the PSD of the output mode over a $\Delta\nu = 400$ MHz bandwidth centered around ν_{conv}. We also measure the inelastic reflection, i.e., leakage of the converted signal through the input port, at the same frequency and bandwidth. The input signal can also be reflected (or transmitted) elastically by the sample. We measure these two elastic signals by integrating the PSD of the input (output) mode over a $\delta\nu = 15$ MHz bandwidth around ν to account for phase noise added by the device. Note that, before integration, the PSD of the spontaneous emission is first subtracted from the desired signals and that the PSDs are divided by $h\nu$ to obtain PSDs in terms of photon rate densities, as in Fig. 2.

To obtain the probabilities corresponding to those different outcomes, the photon rates obtained after integration of the different PSDs are divided by the photon rate we apply at the input of the device. In the case of the converted signals, the result is divided by n to account for multiplication. The input rate is calibrated by applying a microwave signal at frequency ν and integrating the PSD reflected by the sample biased at $\Phi = \Phi_0/2$ and $\nu_J = 2$ GHz, where it is essentially elastically reflecting all the input power (see Appendix B for more details on the calibration).

These probabilities are presented in Fig. 3, where the input frequency ν is chosen to obtain a maximum of conversion. The input power is kept low to have, on average, less than one photon in the input mode. The three conversion probabilities (Fig. 3, orange curves) reach a well-defined maximum as a function of flux, indicated by vertical dashed lines. At this point, the conversion rate matches the loss rate of the input mode, leading to destructive interference in elastic reflection. This situation corresponds to $|\epsilon_n| = 1$ in Eq. (1). With increasing n, the position of this maximum shifts toward lower fluxes in the SQUID loop, thus higher Josephson energies. This behavior is well explained by Eq. (2) because $g_{out} < 1$.

Ideally, at this point the conversion probability should be 1 and the reflection probability 0 [see Eq. (1)]. For the $n = 1$ case, Fig. 3(a), this is almost the case: At $\Phi = 0.47\Phi_0$, the conversion probability reaches 0.90 while the reflection probability drops below 10^{-2}. For $n = 2$ at $\Phi = 0.39\Phi_0$, the conversion probability reaches 0.73 while the reflection probability is still low at 0.018. For $n = 3$ at $\Phi = 0.28\Phi_0$, the conversion probability reduces to 0.69 while the reflection probability increases to 0.20, due to an increase and a shift of the minimum of reflection.

The sum of the probabilities of the four processes we monitor is close to 1 at low Josephson energy (flux close to $\Phi_0/2$), indicating that elastic scattering and the desired conversion process fully explain the behavior of our device. At larger Josephson energies it drops significantly
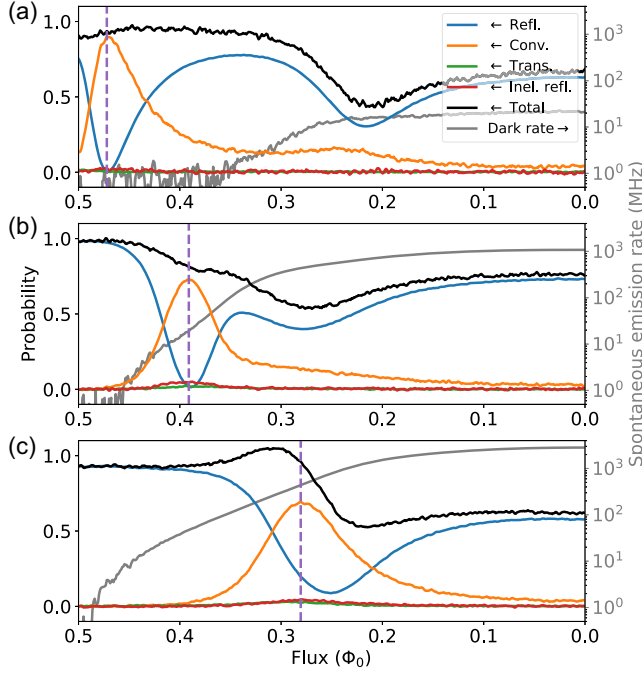
FIG. 3. Reflection, conversion, transmission, and inelastic reflection probabilities as well as spontaneous emission for $n = 1$ (a), 2 (b), and 3 (c) as a function of flux in the SQUID loop. The vertical dashed lines represent the flux values at which the conversion probabilities are highest. In (a), the input frequency is 4.773 GHz and the bias voltage is 1.30 GHz. In (b), the input frequency is 4.71 GHz and the bias voltage is 7.37 GHz. In (c), the input frequency is 4.74 GHz and the bias voltage is 13.37 GHz. For these three plots, the input power of -127 dBm is chosen to have less than one photon on average in the input resonator.

below 1. The missing signal is likely converted to unmonitored frequencies: with increasing Josephson energy new processes involving several Cooper pairs and photons in different spurious modes of the circuit become important [28]. Especially low-frequency modes, even if they have low quality factor and low characteristic impedance, may then be strongly driven by the Josephson junction and take away arbitrary energy from the conversion process. As seen in Fig. 2, those processes are quite difficult to identify from the measurement background when the Josephson energy and the bias voltage increase. In the $n = 3$ case we also see the sum of probabilities exceed 1 just before the maximum of conversion, indicating an energy imbalance between photon input and the monitored processes. We attribute this extra signal to spurious amplification of the input mode prior to photomultiplication. Indeed, the bias condition for $n = 3$ is close to $2eV \approx 3\nu_{\rm in}$, and under this condition a tunneling Cooper pair can spontaneously generate three photons at the input. An incoming photon will accelerate these processes due to stimulated emission, leading to gain, so that it will be amplified before being photomultiplied or reflected (leading to an increase of reflection as seen in Fig. 3). We have

documented a similar amplification process involving two photons [29]. The high spontaneous emission at the $n = 3$ operation point [$\nu_{\rm J} = 13.37$ GHz indicated by the rightmost vertical dashed line in Figs. 2(b) and 2(c)] means that such stimulated emission processes are important.

By changing the input frequency ν as well as the input power, we can obtain the bandwidth and saturation power of the photomultiplier. In Fig. 4, we show those results for $n = 3$. The same curves for $n = 1$ and $n = 2$ can be found in Appendix D. Figure 4(a) shows the reflection and conversion probabilities at low input power, below one photon on average in the input resonator. The maximal conversion efficiency is 0.69 and the full width at half maximum is 116 MHz. This width is set by the bandwidth of the microwave resonators in the setup [17].

In Fig. 4(b) the input power is gradually increased by 3 orders of magnitude. The 1 dB compression point is -119 dBm, corresponding to an approximate photon input rate of 400 MHz. As the power increases, the shape of the curve changes drastically: It first splits in two maxima, then it acquires a third maximum. This behavior arises from the higher order terms of the nonlinear Josephson Hamiltonian, which are resonant at the same voltage and modify the conversion rate as a function of power [17].

The main source of noise added by our device is spontaneous emission of photons plotted in gray in
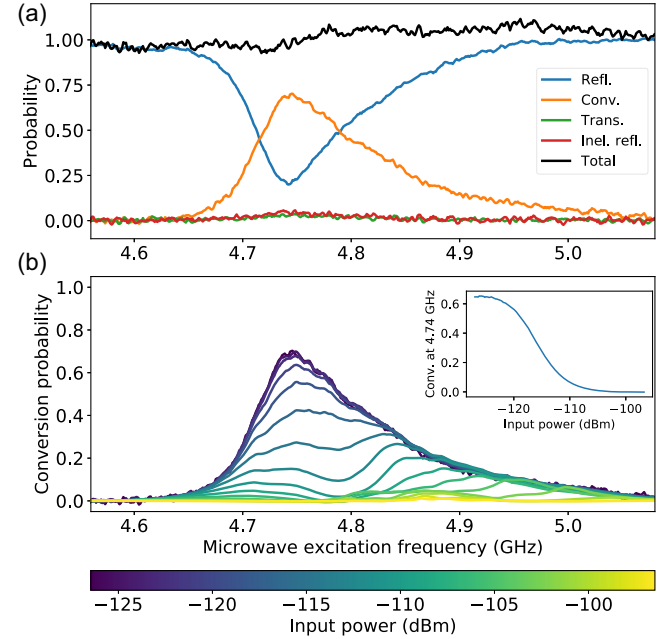

FIG. 4. Bandwidth and saturation power. (a) Reflection, conversion, transmission, and inelastic reflection probabilities for the $n = 3$ process, taken at the flux and voltage values maximizing the conversion probability indicated by a dashed vertical line in Fig. 3(c). The input power is -127 dBm. (b) Conversion probability for the $n = 3$ conversion for various input powers. The inset shows the conversion probability at 4.74 GHz (maximum of conversion at low input power) as a function of input power.

Fig. 3. At the operating point of the $n = 3$ conversion, it is ≈ 400 MHz. It is mainly due to the large Josephson energy required for maximal conversion with our output resonator of characteristic impedance $\approx 400\ \Omega$. As seen in Fig. 2(c), at flux $0.28\Phi_0$ (operation point for the data of Fig. 4), the spontaneous emission background is dominated by higher order processes. An output (and input) mode characteristic impedance closer to $h/(4\pi e^2) \sim 2$ kΩ or a lower bandwidth would require lower Josephson energy for optimal conversion [see Eq. (2)], which would significantly reduce spontaneous emission rates (see Appendix F). At the same time, this lower Josephson energy would also reduce spurious amplification process in the $n = 3$ case (see discussion above on sum of probabilities).

In summary, we have experimentally demonstrated multiplication of the photon number of an incoming microwave signal by an integer factor of 3, with efficiency reaching 0.69. The key characteristics of our device are well understood theoretically [17]. We expect these results to be significantly improved by implementing a better control over the characteristics of our devices, in particular, resonator frequencies and impedances. This would reduce the unwanted processes in our system and significantly lower the observed spontaneous emission rate, which is currently high but qualitatively understood. Cascading two such devices would allow for a photon number gain of $n_{\text{total}} = 3 \times 3$ or more. This gain would then be sufficient to discriminate photon numbers at the input by reading out the photomultiplier with a quantum-limited amplifier [17], and thus detect and count photons. Cascaded photomultipliers followed by linear amplifiers would then implement a photon-number amplifier with minimal added photon noise at the expense of losing, or at least deamplifying, phase information.

R. A. designed and fabricated the device based on an idea by M. H. and performed first measurements. J. G. performed the final measurements, analyzed the data together with R. A. and N. B., and performed simulations. All authors contributed to the experimental setup and calibration methods. F. B. together with R. A., M. H., U. M., and J. G. designed the software for performing the experiment. J. G. wrote the paper together with R. A., M. H., and N. B. and input from all authors.

APPENDIX A: DETAILED EXPERIMENTAL SETUP

The input and output ports of our device are connected to six-port cryogenic switches allowing for *in situ* calibration of the amplification chain (detailed in Appendix B). The common ports of the switches are connected to 0.3–14 GHz cryogenic HEMT amplifiers with noise temperature $T_N \approx 3.5$ K through a 4–8 GHz double-junction circulator on the input side and a 5–12 GHz triple-junction circulator on the output side. The input-side circulator is also connected to a microwave source at room temperature in order to send microwave signals into the device via a line with 90 dB nominal attenuation. At room temperature, the amplified signals are down-converted into the 0–1 GHz band via a custom double-heterodyne receiver, so that both input and output signals can be acquired at the same time by a 2×2 GSa s^{-1} Analog-Digital Converter board.

A dc bias voltage can be applied to the sample via a voltage divider formed by a 1 MΩ resistor at room temperature and a 5 Ω resistor at base temperature. This voltage is then low-pass filtered with a custom filter combining discrete components and a silver-epoxy filter made with superconducting wire for high-frequency filtering (above 10 MHz) and thermalization. This filter is similar to the one used in Ref. [26]. It has a cutoff frequency of 700 Hz and a flat output impedance of 5 Ω up to several hundred MHz. Combined with an on-chip 100 pF capacitor which shorts the signal to the ground at the working frequency, the voltage bias circuit can, therefore, be modeled as as simple RC circuit.

The flux line for the SQUID is biased by a room-temperature voltage source in series with a 5 kΩ resistor. It is filtered at base temperature with a custom Eccosorb filter [27] with a cutoff frequency of the order of 200 MHz.

When measuring our device, we alternate between an "on-state" PSD at the device parameters we want to measure and an "off-state" PSD without voltage bias or input microwave tone. Calculating the difference of these two measurements allows as two accurately subtract the noise of our measurement setup. The PSDs are then calibrated as described in Appendix B.

APPENDIX B: CALIBRATION OF THE AMPLIFICATION CHAIN

To obtain the actual power at the output of our device, we have to calibrate our measurement chain. To do so, for both measurement channels, one cold ($T_C \approx 10$ mK, blue in Fig. 5) and one hot ($T_H \approx 900$ mK, red) 50 Ω resistor are successively connected to the switches. Their thermal noise is then acquired in the 4–8 GHz band. From these two measurements we calculate the gain of the measurement chain from the switches to the digitizer (Y-factor calibration). To ensure correct thermalization of these resistances, they are thermally isolated from the switches via superconducting NbTi coax lines and thermally anchored to, respectively, the mixing chamber stage and the still stage of our dilution refrigerator.
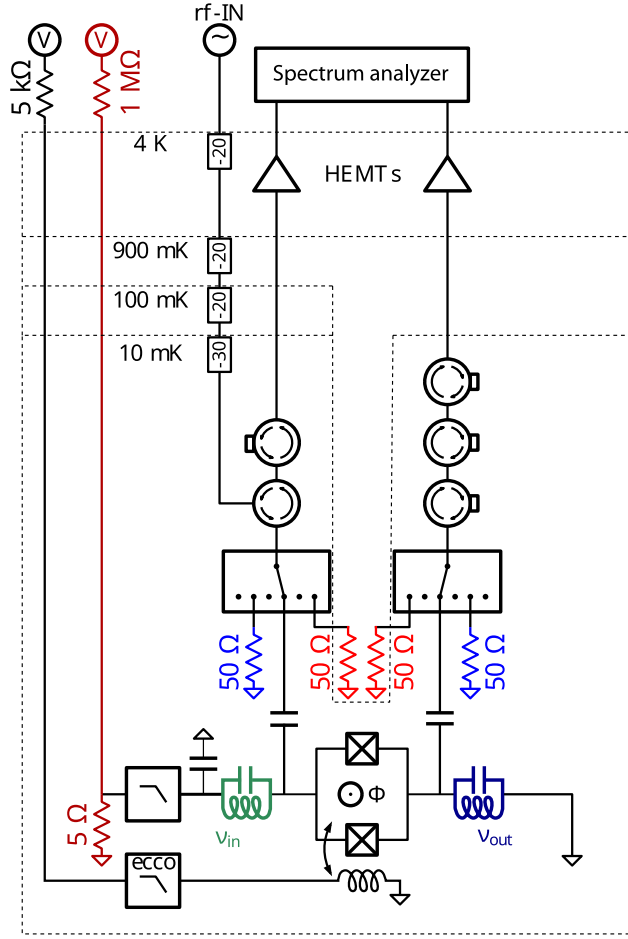
FIG. 5.   Schematics of the experimental setup in the dilution refrigerator.

To calibrate the input line, we perform a reflection measurement with the input switch either on an open port or connected to the cold 50 Ω resistor. This allows us to correct for leakage of the circulators, and gives us the gain of the input line down to the input switch.

We apply a last layer to this calibration by measuring the reflection and the transmission of our device when the bias voltage is far from any working point and the SQUID maximally frustrated. By doing so, we can consider the device as a nondissipative linear component which either reflects or transmits the input signal (at least out of the input resonator bandwidth). This is used to eliminate the contribution of the last cable from the switch to the sample, which we model as a constant attenuation over our frequency window to remove the impact of the input resonator. This correction amounts to 0.267 dB, in agreement with the expected properties of the cable and other measurements done on different samples. This ultimately allows us to compute at each frequency the actual input and output photon rates at the device, which we use to calculate the different probabilities discussed in this work.

APPENDIX C: BIAS VOLTAGE NOISE

In our device, the phase of the input state is transferred to the common phase of the multiphoton output state [17]. In the $n = 1$ case, we thus have phase preservation, and in the $n \neq 1$ case, the phase is spread over several photons. However, this description is correct only if the voltage bias of the Josephson junction is noiseless. In a realistic device such as ours, the voltage bias is quite noisy and its phase has no reference, leading to an effective loss of phase information. To have a better understanding of our device, we have characterized the noise of our voltage bias using the spontaneous emission of the device. Figure 6 shows the PSD of the input and output resonators at maximal SQUID frustration, measured at the resonance frequency of the resonators for a voltage around the process where one Cooper pair gives one photon. In both cases, the width of the measured Lorentzian is 17.5 MHz.

According to the $P(E)$ theory [22,26], this full width at half maximum γ is given by the thermal noise of the low-frequency electromagnetic environment, in this case the bias resistor $R_b = 5$ Ω at electronic temperature T_e:

$$\gamma = \frac{2R_b}{\hbar R_Q} k_B T_e.$$

This allows extracting the effective electronic temperature of the bias resistor. We find $T_e = 86$ mK. However, this value has to be taken with caution, and is likely significantly overestimated because for $P(E)$ to be valid, the electromagnetic environment must stay in thermal equilibrium, which is not a good approximation here: Figure 6 shows that even at maximal frustration of the SQUID, the PSD on resonance is larger than 1 photon, a strong deviation from thermal equilibrium. Under this condition, we expect the Lorentzians to be compressed, leading to an overestimation
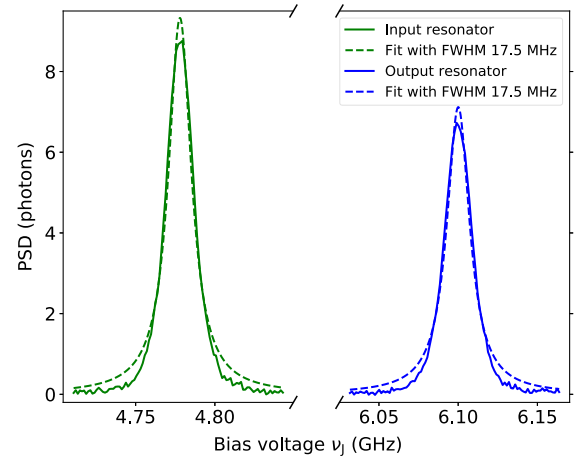

FIG. 6.   Voltage noise. PSD of the input resonator at 4.78 GHz (green) and of the output resonator (blue) at 6.1 GHz, both taken at $\Phi = \Phi_0/2$.

of the temperature of the bias resistor. On devices with lower Josephson energy we indeed observe linewidths corresponding to $T_e \approx 20$–30 mK.

APPENDIX D: RESPONSE AS FUNCTION OF BIAS VOLTAGE

In the main text, we show the response of our device only at the optimal bias point as a function of flux in the SQUID loop in Fig. 3, or frequency in Fig. 4. Figure 7 shows the conversion probability for the $n = 1$ conversion as a function of the input frequency and the bias voltage for several flux values. For values above $0.47\Phi_0$ (Josephson energies below the optimal value), there is one maximum, the amplitude of which increases when the flux approaches $0.47\Phi_0$. Below this value, there are two maxima because the input and output modes enter the strong coupling regime. As SQUID bias is further reduced, the splitting in the anticrossing increases. This behavior is well described by input-output theory applied to the circuit [17]. The dark line with slope 1 (visible at fluxes below $0.46\Phi_0$) in the data of Fig. 7 corresponds to a spurious mode in the junction environment at 3.5 GHz.

Figure 8 shows a fit of the conversion probability for the $n = 1$ conversion to a generalized version of Eq. (1) for slightly off-resonant bias voltage and input frequency, derived in Ref. [17], Sec. III C 1. Instead of fitting a Josephson energy for each flux bias, we use the
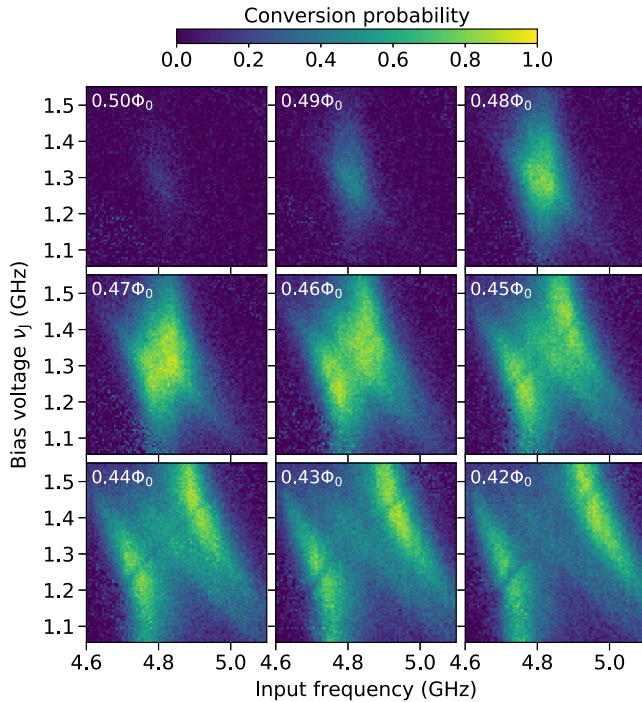

FIG. 7. Measured conversion probability for the $n = 1$ conversion as a function of input frequency and bias voltage for several SQUID flux values. $0.47\Phi_0$ corresponds to the optimal operation point represented by a dashed vertical line in Fig. 3(a).
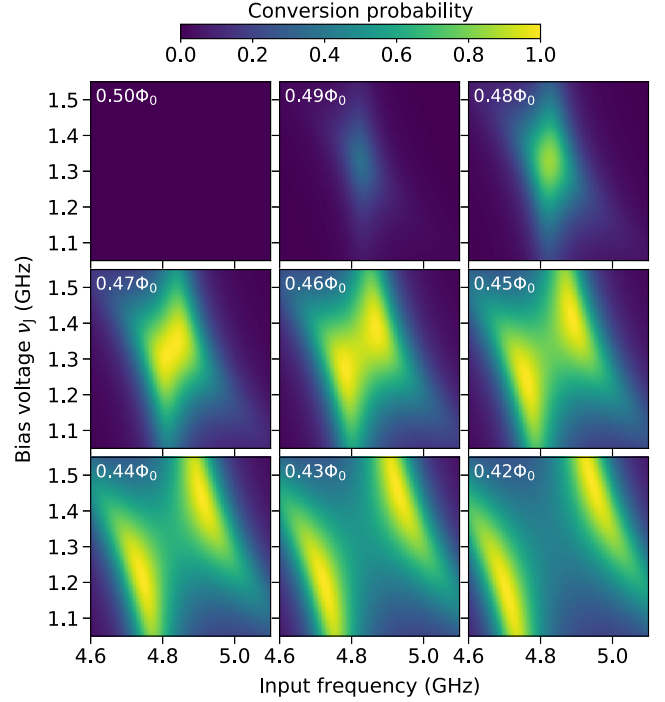

FIG. 8. Fit of the conversion probabilities for $n = 1$ from Fig. 7 to theory [17]. The fit is performed considering $0.47\Phi_0$ to be the ideal matching value of the system (see text).

well-known flux dependence of a symmetric SQUID and the fact that a flux of $0.47\Phi_0$ puts the Josephson energy at its ideal matching value, so that only 1 fitting parameter for Josephson energy is required. Overall, the fits reproduce well our experimental results. The calculation differs from the measurement close to full frustration, because the SQUID is slightly asymmetric, as can be seen in the experimental data for $0.5\Phi_0$ (nonzero conversion and spontaneous emission). The extracted resonance frequencies match well the previously obtained frequencies. The width of the input mode also matches the designed coupling rate, with $\gamma_{in}^{fit} \approx 96$ MHz. However, the result for the width of the output mode $\gamma_{out}^{fit} \approx 226$ MHz differs significantly from the design value. This discrepancy might indicate that the theoretical model is missing part of the behavior of our system. This deviation was also observed in earlier measurement on similar devices [26] and could also be related to the spurious processes observed in Fig. 2, or to the change of optimal input frequency observed in Fig. 3.

APPENDIX E: SATURATION POWER FOR $n = 1$ AND $n = 2$

Figures 9 and 10 show the bandwidth and saturation power of the photomultiplier for the $n = 1$ and $n = 2$ conversion.

Figures 9(a) and 10(a) are taken at low input power, close to one photon on average in the input resonator. They represent the measured reflection, conversion, converted
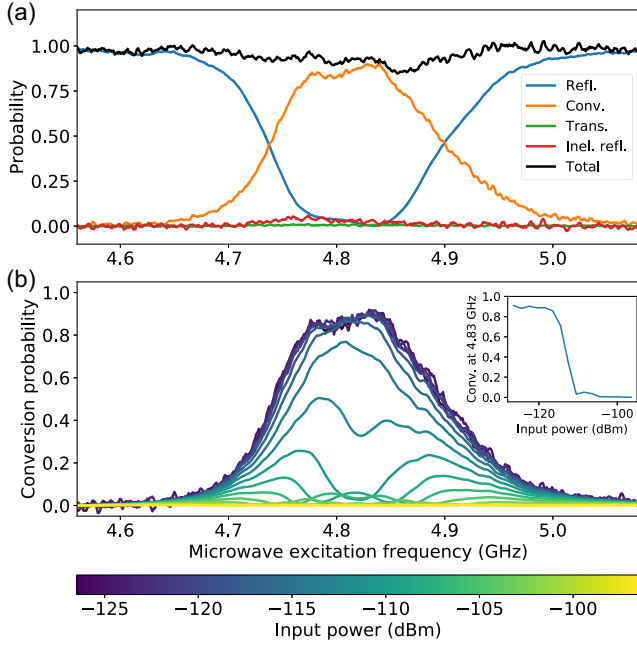
FIG. 9. Bandwidth and saturation power for the $n = 1$ conversion. (a) Reflection, conversion, transmission, and inelastic reflection probabilities taken at the flux value maximizing the conversion probability, indicated by a dashed vertical line in Fig. 3(a). The input power is -127 dBm. (b) Conversion probability for various input powers. The inset shows the conversion probability at 4.84 GHz (maximum of conversion at low input power) as a function of input power.
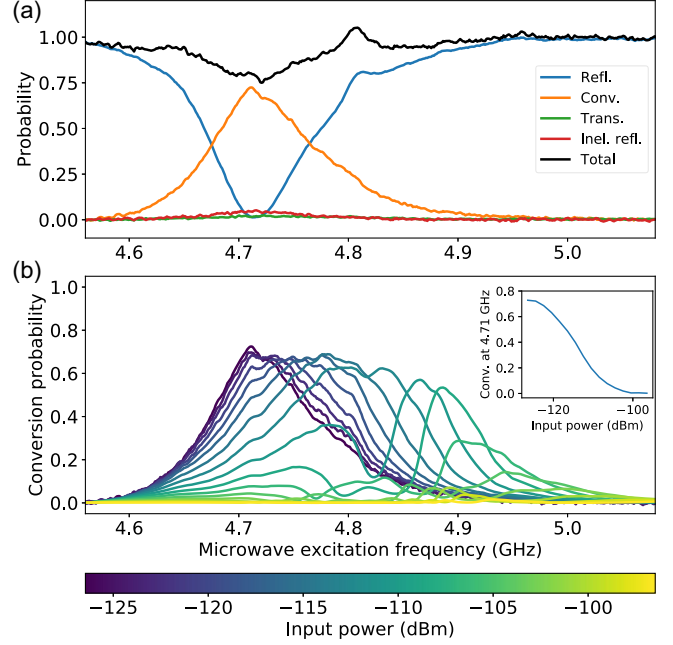
FIG. 10. Bandwidth and saturation power for the $n = 2$ conversion. (a) Reflection, conversion, transmission, and inelastic reflection probabilities taken at the flux value maximizing the conversion probability, indicated by a dashed vertical line in Fig. 3(b). The input power is -127 dBm. (b) Conversion probability for various input powers. The inset shows the conversion probability at 4.71 GHz (maximum of conversion at low input power) as a function of input power.

reflection, and transmission probabilities. For the $n = 1$ conversion, the maximal conversion probability is 0.90, obtained at 4.84 GHz. At this frequency, the reflection probability drops below 10^{-2}, which corresponds to the directivity of our circulators. The bandwidth of this process is 163 MHz. The total probability of the observed processes (black line) stays close to 1 in the whole measurement bandwidth showing that no spurious amplification process is taking place at the same time (see main text). For the $n = 2$ conversion, the maximal conversion only reaches 0.73 at 4.71 GHz with a reflection dropping to 0.018. The bandwidth of this process is 106 MHz. The total probability has a small dip at this frequency, indicating that photons are converted to unmonitored frequencies or that power is dissipated in the device.

In Figs. 9(b) and 10(b), the input power is increased to a few hundred photons on average in the input resonator and the conversion probability is plotted for each input power. The same behavior as for the $n = 3$ conversion [Fig. 4(b)] is observed for the one-to-one conversion [Fig. 9(b)]: Several maxima appear as the power is increased. The 1 dB compression point for the $n = 1$ conversion is -114.5 dBm, corresponding to an input photon rate of approximately 1.1 GHz. The $n = 2$ conversion (Fig. 10) has a slightly different behavior: The frequency at which the maximal conversion probability is observed is shifting

to higher frequencies as the input power is increased. The 1 dB compression point for the $n = 2$ conversion is -118.5 dBm, corresponding to an input photon rate of approximately 440 MHz. Those values are larger than for the $n = 3$ conversion presented in the main text. This is not surprising as the energy in the output mode increases with n for a given input power.

APPENDIX F: UNDERSTANDING AND REDUCING SPONTANEOUS EMISSION

While $P(E)$ theory [22] is barely applicable when we voltage bias our device within one of the two resonators, even at the lowest E_J (see Appendix C), we can use it to estimate the spontaneous emission rate of our device. $P(E)$ gives the probability distribution of a Cooper pair tunneling while emitting the energy E into electromagnetic modes. It is valid when (1) the electromagnetic environment is close to thermal equilibrium and (2) $E_J P(2eV) \ll 1$ [22]. At the working point, outside of any resonator bandwidth, the spontaneous photon emission from the junction is low enough (see Fig. 2) and these two conditions are verified, at least at the lowest E_J. When we tune E_J to obtain the maximum of conversion, the validity conditions remain fulfilled for $n = 1$ and $n = 2$, and reach their limit for $n = 3$. This theory also only describes uncorrelated

tunneling events; higher order processes involving correlated tunneling of two or more Cooper pairs may modify spontaneous emission rates for some voltages [19]. Still, despite its limitations, $P(E)$ theory remains a good tool to explore the general behavior of the spontaneous emission of our device and explore ways to improve it.

Within the limits of $P(E)$ theory, the spontaneous emission rate spectral density is [15]

$$\frac{d\Gamma}{d\nu} = \frac{\pi}{\hbar} E_J^2 \frac{\mathrm{Re}\, Z(\nu)}{\nu R_Q} P(2eV - h\nu).$$

We first compute the electromagnetic environment of the junction, described by an impedance $Z(\nu)$ which we calculate from the frequencies and bandwidths extracted experimentally. From $Z(\nu)$ we numerically calculate $P(E)$ using a finite temperature ($T = 10$ mK) iterative method [30] which allows us to compute $d\Gamma/d\nu$ for each of the three working points discussed in the main text. The Josephson energy is chosen to be the theoretical value leading to a perfect matching for each conversion [see Eqs. (1) and (2)]. As in the main text, the calculated spectral density is integrated over a 400 MHz bandwidth centered over either the input or

output mode to obtain the emission rate of each resonator. These emission rates are shown in Fig. 11 as a function of bias voltage. We can see that the spontaneous emission has a similar behavior as the one observed experimentally (see Fig. 2), with less overall spurious peaks, because $Z(\nu)$ we use for these calculations does not include any spurious resonances caused by the measurement setup. Note that for the $n = 3$ case, the model is not applicable as soon as the voltage reaches the first mode, around 4.5 GHz. However, the order of magnitude for the spontaneous emission is still close to the experimental results.

$P(E)$ theory does not take into account that a photon emitted into the input mode may be converted to n photons in the output mode in a second, correlated, tunneling event. In order to properly estimate the total output spontaneous emission rate Γ, we sum up the weighted spontaneous emission from the input and output modes: $\Gamma = \Gamma_{\mathrm{out}} + (n/2)\Gamma_{\mathrm{in}}$. The $n/2$ factor comes from the perfect matching condition, causing half of the photons coming from the input mode to be converted and the other half to leak through the input line. These expected total spontaneous emission rates are written in Fig. 11 for each process and are close to the experimentally measured rates
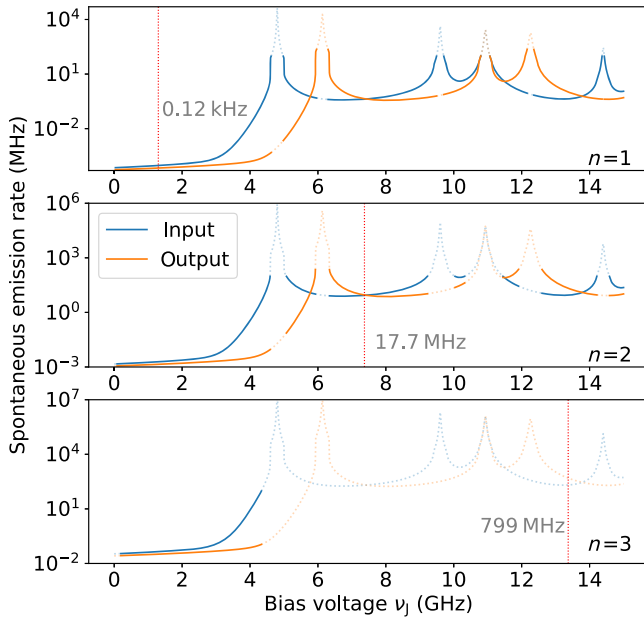

FIG. 11. Partial spontaneous emission from the input or output resonator of our device as a function of the bias voltage, at $T = 10$ mK, calculated using $P(E)$ theory with $f_{\mathrm{in}} = 4.8$ GHz, $f_{\mathrm{out}} = 6.13$ GHz, $Z_c^{\mathrm{in}} = Z_c^{\mathrm{out}} \approx 400\,\Omega$, $\gamma_{\mathrm{in}} = 96$ MHz, and $\gamma_{\mathrm{out}} = 226$ MHz. E_J is chosen to be the theoretical value for perfect matching for each conversion process. The dashed lines indicate the nonapplicability of the theoretical model (see main text). The vertical dashed red lines indicate the voltage bias used for the given conversion process, and the rates written in gray correspond to the expected total spontaneous emission rate at the operating point.
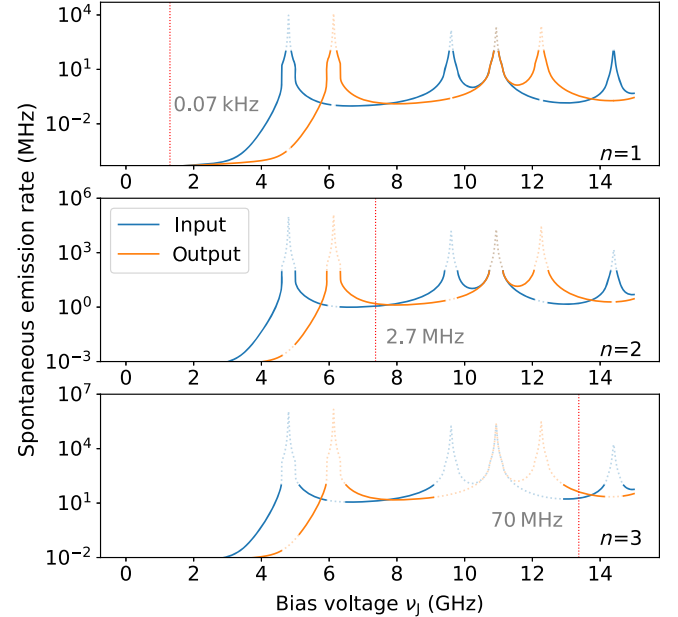
FIG. 12. Partial spontaneous emission from the input or output resonator of a hypothetical device as a function of the bias voltage, at $T = 10$ mK, calculated using $P(E)$ theory with $f_{\mathrm{in}} = 4.8$ GHz, $f_{\mathrm{out}} = 6.13$ GHz, $Z_c^{\mathrm{in}} = 600\,\Omega$ $Z_c^{\mathrm{out}} = 800\,\Omega$, $\gamma_{\mathrm{in}} = 96$ MHz, and $\gamma_{\mathrm{out}} = 100$ MHz. E_J is chosen to be the theoretical value for perfect matching for each conversion process. The dashed lines indicate the nonapplicability of the theoretical model (see main text). The vertical dashed red lines indicate the voltage bias used for the given conversion process, and the rates written in gray correspond to the expected total spontaneous emission rate at the operating point.

(see Fig. 3) for $n = 1$ and $n = 2$, and still of the same order of magnitude for $n = 3$. Note that Γ_{out} has weaker bunching than the multiplied photons. This could be important for estimating the dark count rates if the photomultiplier is used in a thresholding measurement.

In order to reduce those rates, several changes can be implemented. The most straightforward change would be to increase the characteristics impedance of the modes. This would increase the spontaneous emission when biased on resonance, but the reduction in E_J [see Eq. (2)] needed for our processes would reduce the overall emission when biased outside of the resonators, which is the case for all working points in the main text. Another change would be to reduce the bandwidths, which would again reduce the required Josephson energy and thus reduce the spontaneous emission. If we increase the values for Z_c and reduce γ_{out} to its original design value around 100 MHz, we obtain the results in Fig. 12. With those parameters, we can see that the system is more in the applicability range of the $P(E)$ theory. The total spontaneous emission rate of this hypothetical device would be one order of magnitude lower than the total spontaneous emission rate of our current device.

Figure 12 shows that even more significant reductions in spontaneous emission rate can be achieved when the Josephson frequency is kept lower than the input and output mode frequency where spontaneous emission is thermally activated and, therefore, strongly suppressed at dilution temperatures.

[1] Y. F. Chen, D. Hover, S. Sendelbach, L. Maurer, S. T. Merkel, E. J. Pritchett, F. K. Wilhelm, and R. McDermott, *Microwave photon counter based on Josephson junctions*, Phys. Rev. Lett. **107**, 217401 (2011).

[2] S. Kono, K. Koshino, Y. Tabuchi, A. Noguchi, and Y. Nakamura, *Quantum non-demolition detection of an itinerant microwave photon*, Nat. Phys. **14**, 546 (2018).

[3] J. C. Besse, S. Gasparinetti, M. C. Collodo, T. Walter, P. Kurpiers, M. Pechal, C. Eichler, and A. Wallraff, *Single-shot quantum nondemolition detection of individual itinerant microwave photons*, Phys. Rev. X **8**, 021003 (2018).

[4] B. Royer, A. L. Grimsmo, A. Choquette-Poitevin, and A. Blais, *Itinerant microwave photon detector*, Phys. Rev. Lett. **120**, 203602 (2018).

[5] R. Lescanne, S. Deléglise, E. Albertinale, U. Réglade, T. Capelle, E. Ivanov, T. Jacqmin, Z. Leghtas, and E. Flurin, *Irreversible qubit-photon coupling for the detection of itinerant microwave photons*, Phys. Rev. X **10**, 021038 (2020).

[6] A. L. Grimsmo, B. Royer, J. M. Kreikebaum, Y. Ye, K. O'Brien, I. Siddiqi, and A. Blais, *Quantum metamaterial for broadband detection of single microwave photons*, Phys. Rev. Appl. **15**, 034074 (2021).

[7] P. L. Richards, *Bolometers for infrared and millimeter waves*, J. Appl. Phys. **76**, 1 (1994).

[8] B. S. Karasik, A. V. Sergeev, and D. E. Prober, *Nanobolometers for THz photon detection*, IEEE Trans. THz Sci. Technol. **1**, 97 (2011).

[9] G. Lee, D. K. Efetov, W. Jung, L. Ranzani, E. D. Walsh, T. A. Ohki, T. Taniguchi, K. Watanabe, P. Kim, D. Englund, and K. C. Fong, *Graphene-based Josephson junction microwave bolometer*, Nature (London) **586**, 42 (2020).

[10] B. Yurke, L. R. Corruccini, P. G. Kaminsky, L. W. Rupp, A. D. Smith, A. H. Silver, R. W. Simon, and E. A. Whittaker, *Observation of parametric amplification and deamplification in a Josephson parametric amplifier*, Phys. Rev. A **39**, 2519 (1989).

[11] N. Bergeal, F. Schackert, M. Metcalfe, R. Vijay, V. E. Manucharyan, L. Frunzio, D. E. Prober, R. J. Schoelkopf, S. M. Girvin, and M. H. Devoret, *Phase-preserving amplification near the quantum limit with a Josephson ring modulator*, Nature (London) **465**, 64 (2010).

[12] C. Macklin, K. O'Brien, D. Hover, M. E. Schwartz, V. Bolkhovsky, X. Zhang, W. D. Oliver, and I. Siddiqi, *A near–quantum-limited Josephson traveling-wave parametric amplifier*, Science **350**, 307 (2015).

[13] H. A. Haus and J. A. Mullen, *Quantum noise in linear amplifiers*, Phys. Rev. **128**, 2407 (1962).

[14] C. M. Caves, *Quantum limits on noise in linear amplifiers*, Phys. Rev. D **26**, 1817 (1982).

[15] M. Hofheinz, F. Portier, Q. Baudouin, P. Joyez, D. Vion, P. Bertet, P. Roche, and D. Esteve, *Bright side of the Coulomb blockade*, Phys. Rev. Lett. **106**, 217005 (2011).

[16] J. R. Souquet and A. A. Clerk, *Fock-state stabilization and emission in superconducting circuits using dc-biased Josephson junctions*, Phys. Rev. A **93**, 060301(R) (2016).

[17] J. Leppäkangas, M. Marthaler, D. Hazra, S. Jebari, R. Albert, F. Blanchet, G. Johansson, and M. Hofheinz, *Multiplying and detecting propagating microwave photons using inelastic Cooper-pair tunneling*, Phys. Rev. A **97**, 013855 (2018).

[18] J. Leppäkangas and M. Marthaler, *Inelastic scattering of microwave radiation in the dynamical Coulomb blockade*, Phys. Rev. B **98**, 224511 (2018).

[19] C. Rolland, A. Peugeot, S. Dambach, M. Westig, B. Kubala, Y. Mukharsky, C. Altimiras, H. le Sueur, P. Joyez, D. Vion, P. Roche, D. Esteve, J. Ankerhold, and F. Portier, *Antibunched photons emitted by a dc-biased Josephson junction*, Phys. Rev. Lett. **122**, 186804 (2019).

[20] A. Peugeot, G. Ménard, S. Dambach, M. Westig, B. Kubala, Y. Mukharsky, C. Altimiras, P. Joyez, D. Vion, P. Roche, D. Esteve, P. Milman, J. Leppäkangas, G. Johansson, M. Hofheinz, J. Ankerhold, and F. Portier, *Generating two continuous entangled microwave beams using a dc-biased Josephson junction*, Phys. Rev. X **11**, 031008 (2021).

[21] G. C. Ménard, A. Peugeot, C. Padurariu, C. Rolland, B. Kubala, Y. Mukharsky, Z. Iftikhar, C. Altimiras, P. Roche, H. le Sueur, P. Joyez, D. Vion, D. Esteve, J. Ankerhold, and F. Portier, *Emission of photon multiplets by a dc-biased superconducting circuit*, Phys. Rev. X **12**, 021006 (2022).

[22] G.-L. Ingold and Y. V. Nazarov, *Charge tunneling rates in ultrasmall junctions*, in *Single Charge Tunneling: Coulomb Blockade Phenomena in Nanostructures*, edited by H. Grabert and M. H. Devoret, NATO Advanced Studies Institute, Ser. B, Vol. 294 (Plenum, New York, 1992), Chap. 2, pp. 21–107.

[23] T. Holst, D. Esteve, C. Urbina, and M. H. Devoret, *Effect of a transmission line resonator on a small capacitance tunnel junction*, Phys. Rev. Lett. **73,** 3455 (1994).

[24] B. Peaudecerf, T. Rybarczyk, S. Gerlich, S. Gleyzes, J. M. Raimond, S. Haroche, I. Dotsenko, and M. Brune, *Adaptive quantum nondemolition measurement of a photon number*, Phys. Rev. Lett. **112,** 080401 (2014).

[25] A. Essig, Q. Ficheux, T. Peronnin, N. Cottet, R. Lescanne, A. Sarlette, P. Rouchon, Z. Leghtas, and B. Huard, *Multiplexed photon number measurement*, Phys. Rev. X **11,** 031045 (2021).

[26] R. Albert, *Multiplication of microwave photons via inelastic Cooper pair tunneling*, Ph.D. thesis, Université Grenoble Alpes, 2019.

[27] A. Paquette, J. Griesmar, G. Lavoie, R. Albert, F. Blanchet, A. Grimm, U. Martel, and M. Hofheinz, *Absorptive filters for quantum circuits: Efficient fabrication and cryogenic power handling*, Appl. Phys. Lett. **121,** 124001 (2022).

[28] S. Meister, M. Mecklenburg, V. Gramich, J. T. Stockburger, J. Ankerhold, and B. Kubala, *Resonators coupled to voltage-biased Josephson junctions: From linear response to strongly driven nonlinear oscillations*, Phys. Rev. B **92,** 174532 (2015).

[29] S. Jebari, F. Blanchet, A. Grimm, D. Hazra, R. Albert, P. Joyez, D. Vion, D. Estève, F. Portier, and M. Hofheinz, *Near-quantum-limited amplification from inelastic Cooper-pair tunnelling*, Nat. Electron. **1,** 223 (2018).

[30] G.-L. Ingold and H. Grabert, *Finite-temperature current-voltage characteristics of ultrasmall tunnel junctions*, Europhys. Lett. **14,** 371 (1991).

Correction: An invalid version of Fig. 1 was used for publication and has been replaced with the correct version.